INT. J. REMOTE SENSING, 1999, VOL. 20, NO. 17, 3273–3280

A new method for high accuracy navigation of NOAA AVHRR imagery

A. R. S. MARÇAL
Department of Applied Physics and Electronic & Mechanical Engineering, University of Dundee, Dundee DD1 4HN, Scotland, UK

(*Received 5 February 1997; in final form 16 July 1998*)

Abstract. A method to produce rectified Advanced Very High Resolution Radiometer (AVHRR) datasets is proposed, using both the orbital model and identification of ground control points (GCPs), involving a single image transformation from the raw imagery. The ability of the orbital model to determine the geographical co-ordinates of pixels in a raw AVHRR image was tested, using a total of 1098 GCPs in 24 AVHRR images. Five of the 24 images were also rectified using the method proposed, using a newly identified set of GCPs. The differences between the geographical co-ordinates of the existing GCPs and those determined by the new method are calculated and discussed.

1. Introduction

The Advanced Very High Resolution Radiometer (AVHRR), onboard the National Oceanic and Atmospheric Administration (NOAA) polar orbital satellites, provide daily coverage of the Earth. Various applications of AVHRR data require the imagery to be geometrically corrected and projected into geographical co-ordinates. This process of navigation of satellite data provides map-like imagery that can be used for temporal analysis.

Several fully or nearly automatic methods for navigating AVHRR imagery, based on the satellite trajectories, have been proposed (Brush 1985, Brunel and Marsouin 1987, Ho and Asem 1986, Cracknell and Paithoonwattanakij 1989, Marsouin and Brunel 1991, Bachmann and Bendix 1992), with accuracy of around 1–2 km. The automatically produced images have a low frequency error component, mainly due to timing errors and the orbital elements and models, and a high frequency error component, due to variations in the sensor's attitude—roll, pitch and yaw (Krasnopolsky and Breaker 1994). The low frequency error can easily be removed by a constant shift of the image co-ordinates. To remove the high frequency error, and therefore achieve higher accuracy in the registration process, it is necessary to use ground control points (GCPs), i.e. unique geographical locations or features such as small islands, lakes, capes, etc. (Krasnopolsky and Breaker 1994), for each of which the location in the image can be identified and the location on a map is known. The identification of GCPs is a time-consuming task, and may itself introduce a further source of error due to uncertainty in identifying the exact location of a particular feature on a satellite image. For high accuracy a large number of GCPs

International Journal of Remote Sensing
ISSN 0143-1161 print/ISSN 1366-5901 online
http://www.tandf.co.uk/JNLS/res.htm
http://www.taylorandfrancis.com/JNLS/res.htm

need to be used. In the past, attempts have been made to reduce the required number of GCPs by first using the orbital parameters to obtain an approximate rectification and then using a small number of GCPs to refine the results to give the accuracy required (Illera *et al.* 1996).

This paper has two objectives: (i) to investigate the orbital model ability to calculate geographical co-ordinates of a pixel of a raw AVHRR image; and (ii) to present a new rectification method, allowing for sub-pixel accuracy to be achieved. The rectification method presented uses both the orbital model and GCPs to establish a single image transformation from raw to final image. The method was developed with the aim of 'near real time' processing of AVHRR data for applications which require high rectification accuracy in a regional context. It is currently being used at the University of Dundee to produce 1 km resolution Normalized Difference Vegetation Index (NDVI) maximum value composites and weekly snow cover composites (Marçal and Slater 1997).

2. New image rectification method

The method described here was developed at the University of Dundee, using UNIX C programs and PCIWorks scripts (PCI 1996). The system was developed to allow the easy identification of GCPs using PCI-GCPWorks, but it can be easily adapted to allow the use of other software packages for the identification of GCPs.

2.1. *Orbital model*

The orbital model used is based on a spherical Earth and a circular orbit (Brush 1982, 1985, Ho and Asem 1986). The latitude (Φ) and longitude (λ) of a raw image co-ordinate are obtained from equations (1) and (2),

$$\Phi = \sin^{-1}(\cos G \sin\theta \sin\gamma + \cos\gamma \sin G) \tag{1}$$

$$\lambda = \cos^{-1}\left(\frac{\cos G \cos\theta}{\cos\Phi}\right) + K'\theta + L_{eq} \tag{2}$$

where γ is the satellite inclination to the polar axis, θ the geocentric angle transversed from the equator, L_{eq} the longitude of equator crossing, and K' is the Earth rotation constant. The geocentric angle (G) is obtained from equation (3),

$$G = \sin^{-1}\left[\left(1 + \frac{h}{R}\right)\sin M\right] - M \tag{3}$$

where M is the sensor mirror angle, R the Earth radius, and h the satellite height.

The geographic area of interest and georeferenced image characteristics are predefined. For the Scotland images tested an area of 380 km by 530 km was defined, with the top left corner set to 50 000 easting and 1060 000 northing on a British National Grid (BNG) map projection, and 1 km pixel size. A set of control points is produced automatically (ACPs) on the AVHRR raw image. An initial step increment is computed for the area of interest (31 pixels for the example referred). The orbital model is used to calculate geographical co-ordinates of raw image pixels, sampled with the step increment. A pixel is rejected when the calculated geographic co-ordinates fall outside the area of interest plus a small margin (20 km for the example referred). The step increment is reduced by one until the number of ACPs accepted reach 256. This limit is imposed by the PCI algorithms used. The final set of ACPs will have about 250 equally spread ACPs on the interest area, regardless of the area covered by the raw AVHRR image.

2.2. *Combined orbital model and GCP based rectification*

A polynomial transformation (**f**), of order F, is performed on the original image, using a least square fit on the set of ACPs to obtain the polynomial coefficients. A georeferenced dataset covering the pre-defined area of interest is produced. A set of GCPs is then inserted manually on this dataset, using for example a digital map with PCI-GCPWorks software. A grey scale or an RGB image, combining any available AVHRR channel or NDVI, can be used to identify GCPs. Various enhancement modes and zooming ranges are available within PCI-GCPWorks. Units of 1/10 of a pixel can be used (corresponding to about 100 m for AVHRR data), allowing for sub-pixel accuracy to be achieved in suitable areas.

The set of GCPs identified manually is used to determine the parameters of a polynomial transformation (**g**), of order G, between the automatically produced image and a digital map. The original set of ACPs is altered, using the polynomial transformation (**g**) to change the geographical co-ordinates of the ACPs. This new set of control points is used to obtain a polynomial transformation ($\mathbf{h} = \mathbf{g}\circ\mathbf{f}$; $\mathbf{h}(x, y) = \mathbf{g}(\mathbf{f}(x, y))$, which is used to rectify the raw image into a final georeferenced dataset. Figure 1 is a diagram of the whole process. The final imagery is produced by a single polynomial transformation from the original raw data. The image smoothing due to resampling is minimized as there is only one image transformation between the raw and the final imagery. The order (H) of the polynomial **h** is $H = \text{Max.}\{G, F, G.F\}$. Using a third-order polynomial for the orbital model transformation of the raw image (**f**) and a first-order polynomial transformation between the automatically produced image and the digital map (**g**), the final transformation (**h**) polynomial order will be 3.

3. AVHRR orbital model test

3.1. *Methodology*

GCPs were inserted in 24 NOAA-14 AVHRR images of Scotland, by identifying similar features on the raw satellite image and on a high accuracy digital map (125 m pixel, 60 m maximum error). For each GCP there is a pair of geographical co-ordinates

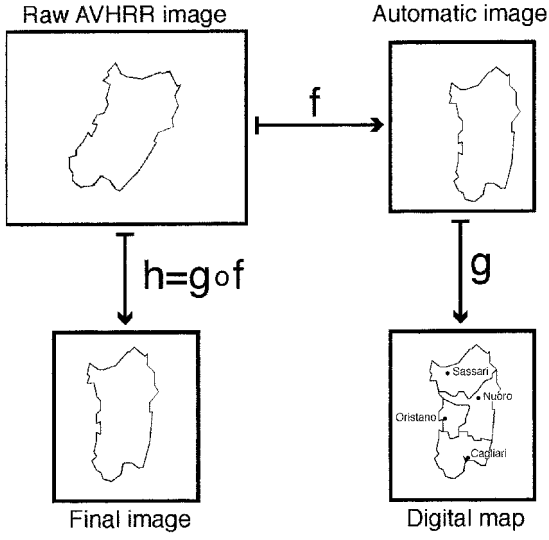

Figure 1. Overview of the new rectification method.

(easting, northing) with an associated pair of raw image co-ordinates (pixel, line). The distinctive coastline of Scotland made it generally possible, except in the presence of clouds, to insert a large number of well-distributed GCPs on each raw satellite image (between 36 and 51 GCPs on each image, 1098 GCPs in total). The AVHRR images tested are subsections of 500 by 500 pixels or 1000 by 1000 pixels, with various viewing geometry conditions. The image size, viewing geometry and number of GCPs on each image are presented in table 1. The minimum and maximum satellite viewing angles were calculated for the area of interest (Scotland), as only this area was used for GCPs. Great care was taken in the identification of GCPs, which were all double checked using PCI-GCPWorks software. Using a third-order polynomial transformation, the highest root mean square error in a GCP was 0.35 km (Marçal and Wright 1997).

For each GCP available, the latitude and longitude of the raw co-ordinates (pixel, line) were calculated using the orbital model. The latitude and longitude co-ordinates were converted to BNG easting and nothing (Ordnance Survey 1995), which were compared to the GCP geographical co-ordinates. Each AVHRR raw image was processed independently, using the corresponding orbital parameters of the image acquisition day.

3.2. *Results*

The results of the comparison between the orbital model calculated co-ordinates and the GCP co-ordinates are presented in table 2, for each of the 24 images studied. The mean difference in easting, ΔE, and northing, ΔN, between the orbital co-ordinates

Table 1. Description of the 24 AVHRR images used for the orbital model test.

AVHRR sub-scene characteristics				Number of GCPs	Satellite view angle (°)	
No.	Date	Time	Size		Minimum	Maximum
1	12 Apr 95	1302	500× 500	47	– 12.5	+ 14.5
2	13 Apr 95	1251	500× 500	47	– 1.5	+ 25.5
3	1 May 95	1259	1000× 1000	49	– 10.5	+ 16.5
4	3 May 95	1238	1000× 1000	41	+ 7	+ 33.5
5	17 May 95	1328	1000× 1000	42	– 33	– 10.5
6	20 May 95	1255	1000× 1000	50	– 6.5	+ 20.5
7	12 Jun 95	1349	1000× 1000	44	– 43.5	– 26.5
8	15 Jun 95	1316	1000× 1000	38	– 24	+ 3
9	24 Jun 95	1320	1000× 1000	50	– 27.5	– 0.5
10	25 Jun 95	1309	1000× 1000	51	– 17.5	+ 9.5
11	26 Jun 95	1258	1000× 1000	51	– 8	+ 19
12	8 Jul 95	1229	1000× 1000	38	+ 15.5	+ 39
13	22 Jul 95	1319	1000× 1000	39	– 27	– 1.5
14	25 Jul 95	1247	1000× 1000	41	+ 1.5	+ 28.5
15	27 Jul 95	1225	1000× 1000	36	19	+ 42.5
16	30 Jul 95	1333	1000× 1000	49	– 36	– 11
17	1 Aug 95	1312	1000× 1000	48	– 19.5	+ 7.5
18	4 Aug 95	1239	1000× 1000	49	+ 7.5	+ 33
19	9 Aug 95	1326	1000× 1000	50	– 31	– 6.5
20	10 Aug 95	1315	1000× 1000	47	– 22.5	+ 4.5
21	20 Aug 95	1308	1000× 1000	47	– 16.5	+ 10.5
22	14 Sep 95	1339	500× 500	50	– 38	– 16.5
23	26 Sep 95	1310	500× 500	49	– 16	+ 11
24	28 Sep 95	1249	500× 500	45	+ 2.5	+ 29.5

Table 2. Comparison between the orbital model geographical co-ordinates and the GCPs (in kilometres).

Image no.	ΔE	ΔN	σE	σN	σd	δE	δN	δd
1	2.2	– 13.1	0.41	0.43	0.64	1.57	1.28	1.70
2	3.3	– 16.2	0.40	0.41	0.61	1.55	0.85	1.69
3	4.6	– 12.6	0.36	0.41	0.59	0.81	1.15	1.25
4	7.0	– 7.7	0.66	0.47	0.86	1.54	1.20	1.67
5	– 1.1	3.0	0.50	0.24	0.58	0.98	0.95	1.21
6	0.2	5.0	0.46	0.18	0.53	1.03	0.54	1.08
7	– 6.9	11.7	0.76	0.39	0.88	1.32	0.83	1.49
8	– 4.4	15.7	0.84	0.24	0.89	1.66	0.76	1.66
9	– 1.8	10.5	0.24	0.19	0.33	0.65	0.54	0.75
10	– 2.8	14.4	0.30	0.23	0.40	0.72	0.88	0.94
11	– 0.2	5.8	0.73	0.29	0.82	1.50	0.84	1.50
12	2.4	7.7	0.85	0.56	1.08	1.67	1.39	1.90
13	2.6	– 12.6	0.32	0.54	0.67	0.70	1.91	1.91
14	1.6	– 1.8	0.39	0.37	0.61	1.14	0.95	1.15
15	7.6	– 10.9	0.55	0.53	0.82	1.13	1.07	1.52
16	2.4	– 11.5	0.22	0.54	0.62	0.74	1.26	1.27
17	2.9	– 9.9	0.21	0.48	0.55	0.59	1.23	1.24
18	10.0	– 22.9	0.25	0.48	0.58	0.64	1.31	1.32
19	5.2	– 24.5	0.22	0.47	0.55	0.79	1.09	1.18
20	6.5	– 24.2	0.20	0.59	0.66	0.71	1.39	1.42
21	6.1	– 20.9	0.33	0.58	0.73	1.01	1.24	1.38
22	0.3	– 10.2	0.41	0.40	0.63	1.12	1.00	1.22
23	4.3	– 10.2	0.27	0.35	0.50	0.79	0.78	0.86
24	1.5	10.7	0.93	0.34	1.03	1.75	0.85	1.77
Minimum	– 6.9	– 24.5	0.20	0.18	0.33	0.59	0.54	0.75
Maximum	10.0	15.7	0.93	0.59	1.08	1.75	1.91	1.91
Mean			0.42	0.37	0.62	0.96	0.97	1.24

and the GCPs co-ordinates in one image are obtained using equations (4) and (5).

$$\Delta E = \frac{1}{n} \sum_{i=1}^{n} (E^i_{\text{orbital}} - E^i_{\text{GCP}}) \tag{4}$$

$$\Delta N = \frac{1}{n} \sum_{i=1}^{n} (N^i_{\text{orbital}} - N^i_{\text{GCP}}) \tag{5}$$

where E^i_{orbital}, N^i_{orbital} are easting and northing calculated using the orbital model, and E^i_{GCP}, N^i_{GCP} are easting and northing co-ordinates of GCP i of an image with n GCPs. The mean differences between the orbital model and the GCP co-ordinates were found to be, for the 24 images tested, between – 6.9 and 10.0 km for ΔE, and between – 24.5 and 15.7 km for ΔN.

The mean absolute deviations are calculated using equations (6), (7) and (8).

$$\sigma E = \frac{1}{n} \sum_{i=1}^{n} |(E^i_{\text{orbital}} - \Delta E) - E^i_{\text{GCP}}| \tag{6}$$

$$\sigma N = \frac{1}{n} \sum_{i=1}^{n} |(N^i_{\text{orbital}} - \Delta N) - N^i_{\text{GCP}}| \tag{7}$$

$$\sigma d = \frac{1}{n} \sum_{i=1}^{n} \sqrt{(E^i_{\text{orbital}} - \Delta E - E^i_{\text{GCP}})^2 + (N^i_{\text{orbital}} - \Delta N - N^i_{\text{GCP}})^2} \quad (8)$$

The average value for the mean absolute deviation in easting was 0.42 km, ranging from 0.20 to 0.93 km on the 24 images studied. The average value for the mean absolute deviation in northing was 0.37 km, ranging from 0.18 to 0.59 km. The distance mean absolute deviation was between 0.33 km and 1.08 km for the 24 images, 0.62 km on average. The maximum errors of easting (δE), northing (δN) and distance (δd), are also presented in table 2, for each image.

3.3. *Discussion*

The differences between the orbital model calculated co-ordinates and the map co-ordinates, were found to have two distinct components:

(1) An offset error (ΔE, ΔN), generally a few kilometres.
(2) A high frequency error, varying within a single AVHRR image, much smaller in magnitude than the offset error—generally less than 1 km. No spatial relation was found on the distribution of the high frequency error.

The offset error can be removed easily by inserting one or more GCPs, or by using an automatic algorithm (Cracknell and Paithoonwattanakij 1989, O'Brien and Turner 1992). The high frequency error is generally smaller than the pixel size, between 0.33 and 1.08 km for the 24 images studied, but it is harder to remove. The identification of a large number of widespread GCPs is the most efficient way of reducing the high frequency error in an AVHRR image. The use of more elaborate orbital models can produce automatically rectified images which have smaller errors when compared to a map. However, due to an uncertainty of the sensors attitude, the high frequency error will not be significantly reduced (R. J. H. Brush, personal communication).

4. Test of the new rectification method

4.1. *Accuracy of the method*

Five images were selected, from the 24 images previously used, to check the accuracy of this method. The size of two of the images tested was 500 by 500 pixels; the remaining images were 1000 by 1000 pixels. A total of 239 GCPs were tested, between 45 and 51 GCPs on each raw image. The areas tested had satellite viewing angles between $-36°$ and $+29.5°$. Each image was rectified using the method proposed, with a third-order polynomial **f** and a first-order polynomial **g**. The polynomial **g** was obtained from 12 new GCPs inserted on the automatic dataset.

For each GCP on the original raw image $\{(x,y),(E,N)\}$, the absolute deviation between the original geographical co-ordinates (identified on the raw image) and the co-ordinates determined by the new method $\{(x,y),\mathbf{h}(x,y)\}$ were computed. The maximum and mean absolute deviation in easting, northing and distance, are presented in table 3, as well as the root mean square errors for polynomial **g**. The root mean square errors in the determination of **g** coefficients were between 0.093 and 0.202 km. The root mean square errors for polynomial **f** and **h** are negligible (typically below 0.05 km). For the five images tested, the mean absolute deviation in easting and northing between the manually identified GCPs and the co-ordinates calculated by the new method was between 238 and 305 m (402–461 m in distance), as opposed to

Table 3. Comparison between the new method geographical co-ordinates and the GCPs (in kilometres).

Image no.	σE	σN	σd	δE	δN	δd	rms. E	rms. N
1	0.255	0.298	0.428	1.845	1.145	2.015	0.093	0.118
11	0.305	0.286	0.461	0.812	0.854	0.971	0.160	0.131
16	0.252	0.251	0.402	0.957	0.870	1.109	0.144	0.150
21	0.301	0.252	0.428	1.017	0.633	1.091	0.176	0.202
24	0.281	0.238	0.412	1.104	0.773	1.348	0.105	0.138

rms., root mean square.

between 220 and 930 m for the co-ordinates calculated using the orbital model alone (620–1030 m in distance).

The number of GCPs identified on the automatically produced datasets was later increased from 12 to 20 in two of the images tested. The absolute deviations in geographical co-ordinates were computed again. The results obtained using 20 GCPs on the automatic datasets were found to be very similar to the results obtained using only 12 GCPs, the differences in the mean values being less than 4%.

4.2. *Discussion*

The magnitudes of the differences between the geographical co-ordinates of the original GCPs and those determined by the new method (on average 400 m in distance) are within the uncertainty limits for the identification of GCPs on an AVHRR image. It is significant that very similar results were obtained with considerably less operator time (12 GCPs instead of 45 to 51). Regardless of the area covered by the raw AVHRR image, only the pre-defined area of interest is considered for rectification. The very low root mean square errors indicate that the errors due to the polynomial transformations alone are very small. No evidence of any spatial relation on the distribution of errors was found on any of the images tested.

The limitations of this method are mainly the same as other image rectification methods based on GCPs: (i) it is not always possible to identify a reasonable number of widespread GCPs; (ii) the identification of GCPs is a time-consuming process. Both limitations are reduced by this method, as a large number of GCPs is not required. However, if the number of GCPs is very small, the order of the polynomial transformation **g** might have to be zero, which only allows for the offset error of the orbital model rectified image to be removed. The highest accuracy is achieved when a reasonable number of widely distributed GCPs are inserted, allowing for a first- or second-order polynomial transformation between the automatic dataset and the map. This method facilitates the identification of the same features on a satellite image and on a digital map, since the satellite image used to identify GCPs is visually similar to the map, without introducing excessive smoothing due to resampling the original image twice. The final rectified image is a direct transformation from the raw satellite image.

5. Conclusion

An extensive test of the orbital model ability to determine the geographical co-ordinates of a pixel on an AVHRR raw image was performed. From a total of 1098 GCPs, tested on 24 AVHRR images, it was found that the errors on the geographical co-ordinates determined by the orbital model have two components: an offset error,

and a high frequency error. The offset error is typically of a few kilometres. The high frequency error is typically of the size of the AVHRR pixel.

The new method for the rectification of AVHRR imagery proposed uses both the orbital model and GCPs. The method allows for a final rectified image to be produced by a single image transformation on the raw imagery. The orbital model is used to automatically produce a rectified image, where GCPs are inserted. The GCPs are used to adjust the parameters of the initial (automatic) image transformation. The final georeferenced image is produced with a single polynomial transformation from the raw image, with the polynomial coefficients determined by the orbital model adjusted by the identification of GCPs. The system allows for easier identification of GCPs without introducing excessive smoothing due to resampling. The proposed method was tested with five images. It was found that the errors on the images rectified by this method was within the range of uncertainty for identification of GCPs, on average about 400 m in distance (250–300 m in easting and northing).

Acknowledgments

The author wishes to acknowledge the NERC (National Environmental Research Centre), Dundee Satellite Station for providing the AVHRR data and the Portuguese Ministry of Science and Technology (PRAXIS XXI program) for the financial support. The author also wishes to thank Prof. A. P. Cracknell for helpful suggestions regarding the manuscript.

References

Bachmann, M., and Bendix, J., 1992, An improved algorithm for NOAA-AVHRR image referencing. *International Journal of Remote Sensing*, **13**, 3205–3215.

Brunel, P., and Marsouin, A., 1987, An operational method using ARGOS orbital elements for navigation of AVHRR imagery. *International Journal of Remote Sensing*, **8**, 569–578.

Brush, R. J. H., 1982, *A real time data retrieval system for images from polar orbiting satellites*. PhD thesis, University of Dundee.

Brush, R. J. H., 1985, A method for real-time navigation of AVHRR imagery. *IEEE Transactions on Geoscience and Remote Sensing*, **GE-23**, 876–887.

Cracknell, A. P., and Paithoonwattanakij, K., 1989, Pixel and sub-pixel accuracy in geometric correction of AVHRR imagery. *International Journal of Remote Sensing*, **10**, 616–667.

Ho, D., and Asem, A., 1986, NOAA AVHRR image referencing. *International Journal of Remote Sensing*, **7**, 895–904.

Illera, P., Delgado, J. A., and Calle, A., 1996, A navigation algorithm for satellite images. *International Journal of Remote Sensing*, **17**, 577–588.

Krasnopolsky, V. M., and Breaker, L. C., 1994, The problem of AVHRR image navigation revisited. *International Journal of Remote Sensing*, **15**, 979–1008.

Marçal, A. R. S., and Slater, M. T., 1997, A system for near real time processing of NOAA-AVHRR satellite data: application to snow monitoring in Scotland. *Proceedings of the Sixth International Conference on Image Processing and its Applications, Dublin, Ireland, 14–17 July 1997*, pp. 546–550.

Marçal, A. R. S., and Wright, G. G., 1997, The use of 'overlapping' NOAA-AVHRR NDVI Maximum Value Composites for Scotland and initial comparisons with the LCS88 data on a Scottish Regional and District basis. *International Journal of Remote Sensing*, **18**, 491–503.

Marsouin, A., and Brunel, P., 1991, Navigation of AVHRR images using ARGOS or TBUS bulletins. *International Journal of Remote Sensing*, **12**, 1575–1592.

O'Brien, D. M., and Turner, P. J., 1992, Navigation of coastal AVHRR images. *International Journal of Remote Sensing*, **13**, 509–514.

Ordnance Survey, the National Mapping Agency of Great Britain, 1995, National Grid/ETRF89 Transformation Parameters. Geodetic Information Paper No. 2.

PCI, 1996, PCIWorks Reference Manual Version 6.0.1.